Magnetotransport in ferromagnetic Mn_5Ge_3, $Mn_5Ge_3C_{0.8}$, and $Mn_5Si_3C_{0.8}$ thin films

Christoph Sürgers,[1,*] Gerda Fischer,[1] Patrick Winkel,[1] and Hilbert v. Löhneysen[1,2]
[1]*Karlsruhe Institute of Technology, Physikalisches Institut and DFG-Center for Functional Nanostructures, P.O. Box 6980, 76049 Karlsruhe, Germany*
[2]*Karlsruhe Institute of Technology, Institut für Festkörperphysik, P.O. Box 3640, 76021 Karlsruhe, Germany*
(Received 5 June 2014; revised manuscript received 12 September 2014; published 24 September 2014)

The electrical resistivity, anisotropic magnetoresistance (AMR), and anomalous Hall effect of ferromagnetic Mn_5Ge_3, $Mn_5Ge_3C_{0.8}$, and $Mn_5Si_3C_{0.8}$ thin films has been investigated. The data show a behavior characteristic for a ferromagnetic metal, with a linear increase of the anomalous Hall coefficient with Curie temperature. While for ferromagnetic $Mn_5Si_3C_{0.8}$ the normal Hall coefficient R_0 and the AMR ratio are independent of temperature, these parameters strongly increase with temperature for $Mn_5Ge_3C_x$ films. This difference is presumably due to the different lattice parameters and different atomic configurations of the metalloids Ge and Si affecting the electronic band structure. The concomitant sign change of R_0 and the AMR ratio with temperature observed for $Mn_5Ge_3C_x$ films is discussed in a two-current model indicating an electronlike minority-spin transport at low temperatures.

DOI: 10.1103/PhysRevB.90.104421 PACS number(s): 72.15.Eb, 72.80.Ga, 73.50.Jt, 75.47.Np

I. INTRODUCTION

The vision of spintronics—the development of faster and less power-consuming nonvolatile electronics with increased integration density by utilizing the electron's spin degree of freedom—strongly depends on the ability to inject, manipulate, and detect spin-polarized charge carriers in the semiconductor [1–3]. In search of new materials for spintronic applications, a number of ferromagnetic metals and compounds are being explored with the aim to overcome the various obstacles of spin injection and detection in semiconductors, in particular in Si, and in ferromagnet-semiconductor heterostructures. Ferromagnetic silicides or germanides are favorable due to the possible integration into semiconductor Si- and Ge-based electronics and complementary metal-oxide-semiconductor (CMOS) technology [4]. Mn_5Ge_3 films are an example because they can be epitaxially grown on Ge(111) and are ferromagnetic at room temperature with a Curie temperature $T_C = 296$ K [5] close to $T_C = 304$ K of bulk Mn_5Ge_3 [6]. However, for a real device operating at room temperature T_C values well above room temperature are pivotal. This can be achieved, e.g., by inserting carbon atoms into Mn_5Ge_3 [7–9]. Recently, $Mn_5Ge_3C_{0.8}$ has been implemented in MOS capacitors and Schottky diodes on n-Ge to determine work functions and contact resistivities [10]. Furthermore, Mn_5Ge_3/Ge and $Mn_5Ge_3C_{0.8}$/Ge heterostructures are being investigated for potential spintronic applications [11].

A stabilization of ferromagnetic order by carbon has also been established for the prototype material Mn_5Si_3 which orders antiferromagnetically below 100 K but can be driven ferromagnetic by insertion of carbon with $T_C \approx 350$ K for $Mn_5Si_3C_{0.8}$ [12–14]. The high T_C well above room temperature makes this material interesting to study in light of potential applications in combination with silicon, the mainstream semiconductor. A previous electronic-transport study performed on $Mn_5Si_3C_x$ focused on the effect of carbon concentration x and film thickness d on the resistivity, where the carbon-induced disorder gives rise to scattering of electrons by structure-induced two-level systems at low temperatures [13].

Although the structural and magnetic properties of ferromagnetic $Mn_5Si_3C_x$ and $Mn_5Ge_3C_x$ films have been investigated previously, a detailed magnetotransport study of these films is lacking. Such a study yields characteristic electronic-transport parameters like charge-carrier type and density, size of the magnetoresistance (MR), and of the anisotropic magnetoresistance (AMR), which are important in view of future integration of these materials in Si- or Ge-based spintronic devices. The AMR is the difference between the MR when the magnetization M is aligned in the longitudinal (L) or transverse (T) direction with respect to the current, and the magnetic field H is oriented in the plane of the film. In $3d$ transition metals the AMR ratio $(\rho_{\parallel,\mathrm{L}} - \rho_{\parallel,\mathrm{T}})/\rho_{\parallel,\mathrm{T}}$ is usually a few percent and often larger than the ordinary MR which is caused by the Lorentz force acting on the charge carriers and also observed in nonmagnetic metals. Moreover, ferromagnetic metals show an anomalous Hall effect (AHE) which is usually much larger than the ordinary Hall effect. AMR and AHE have been known for almost a century [15–18] and experienced a renaissance in recent years. Both effects are linked by the microscopic electronic properties of the material such as the spin-split band structure, the density of states (DOS), and the spin-orbit interaction. Hence we have conducted a comprehensive investigation of the magnetotransport properties of ferromagnetic $Mn_5Ge_3C_x$ ($x = 0$, 0.8) and $Mn_5Si_3C_{0.8}$ films for temperatures $T = 2$–400 K. In $Mn_5Ge_3C_x$ films we find a strong temperature dependence of the AMR ratio and of the ordinary Hall coefficient R_0 which both change sign from negative to positive with increasing temperature. In contrast, temperature independent positive R_0 and AMR ratio are observed for ferromagnetic $Mn_5Si_3C_{0.8}$. We argue that the difference between the $Mn_5Ge_3C_x$ and $Mn_5Si_3C_{0.8}$ films presumably arises from the variation of the spin-split band structure in these materials due to the different lattice parameters and the atomic configuration of the metalloid constituents Si and Ge, which sensitively affect the electronic and magnetic properties.

*Christoph.Suergers@kit.edu

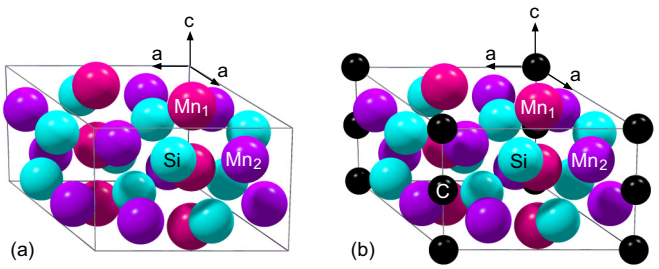

FIG. 1. (Color online) (a) Crystalline structure of Mn_5Si_3. (b) Mn_5Si_3-type structure of Mn_5Si_3C with carbon filling the voids of Mn_2 octahedra at position 2(b) of the space group $P6_3/mcm$. Gray lines indicate the hexagonal unit cell.

A. Materials properties

The prototype phase of the investigated films is the intermetallic compound Mn_5Si_3 with $D8_8$ structure; see Fig. 1(a). The hexagonal unit cell (space group $P6_3/mcm$) contains two formula units with 10 Mn atoms on two inequivalent lattice sites: 4 Mn_1 atoms at position 4(d) (1/3,2/3,0) arranged in chains along the crystallographic c axis, 6 Mn_2 atoms at position 6(g) (y_{Mn},0,1/4) with $y_{Mn} = 0.2358$, and 6 Si atoms at position 6(g) (y_{Si},0,1/4) with $y_{Si} = 0.5991$ [19]. The antiferromagnetic structure of Mn_5Si_3 has been determined by neutron diffraction [20–22] uncovering a noncollinear spin structure below 68 K which gives rise to a topological Hall effect [23]. For the carbon doped samples previous structural analysis suggests that the carbon atoms are arranged in chains by incorporation into the interstitial voids at position 2(b) (0,0,0) of the Mn_2 octahedra [24]; see Fig. 1(b). Inserting carbon atoms to yield $Mn_5Si_3C_x$, gives rise to an anisotropic modification of the local structure around the Mn sites and induces ferromagnetic order with a maximum $T_C = 352$ K for $x = 0.8$ [12,25]. Site-dependent magnetic moments averaging to $1.19\mu_B$/Mn have been inferred for ferromagnetic Mn_5Si_3C from *ab initio* calculations and a local moment of $1.9\mu_B$ attributed to Mn_2 has been observed by broadband nuclear magnetic resonance [26].

The isostructural Mn_5Ge_3 compound with $y_{Mn} = 0.239$ and $y_{Si} = 0.603$ is ferromagnetic with a Curie temperature $T_C = 304$ K [6,27]. *Ab initio* calculations indicate the presence of two competing magnetic phases, a collinear phase and a phase with small noncollinearity [28]. The ferromagnetic stability can be enhanced by carbon insertion [7,9,29] possibly due to a 90° ferromagnetic superexchange mediated by C [8]. A substantial modification of the electronic band structure due to carbon was also derived from a comparison of the T_C dependence on the unit-cell volume for $Mn_5Si_3C_x$ and $Mn_5Ge_3C_x$ [14]. In polycrystalline films, a maximum $T_C \approx 450$ K was reached for $Mn_5Ge_3C_{0.8}$ [7,29]. For higher x, T_C and the magnetization decrease due to the formation of additional phases. A similar C-induced effect was observed for epitaxially grown $Mn_5Ge_3C_x$ films on Ge (111) substrates with $T_C = 430$–450 K for $x \approx 0.7$–0.8, making the material an interesting candidate for potential spintronic applications [9,11]. Table I shows the structural parameters of the materials investigated in this work.

TABLE I. Structural parameters: lattice constants a, c, and unit-cell volume V_{uc}.

	a (Å)	c (Å)	c/a	V_{uc} (Å^3)	Ref.
Mn_5Ge_3 (bulk)	7.184	5.053	0.703	225	[52]
Mn_5Ge_3 (film)	7.157	5.038	0.704	223	[53]
$Mn_5Ge_3C_{0.8}$ (film)	7.135	4.996	0.700	220	[7]
$Mn_5Si_3C_{0.8}$ (film)	6.939	4.831	0.696	201	[12]

B. Anomalous Hall effect

The electrical resistivity $\rho = Vwd/LI$ of a film of thickness d and width w is determined from the longitudinal voltage V measured along a stripe of length L with current I. The Hall effect is measured as transverse voltage V_{xy} to the current I in perpendicular magnetic field H, where the Hall resistivity is obtained via $\rho_{xy} = V_{xy}d/I$. In ferromagnetic materials, the Hall effect comprises the ordinary term ρ_{xy}^0 arising from the Lorentz force acting on the charge carriers, and the extraordinary or anomalous term ρ_{xy}^{AH} due to the magnetization M [15]:

$$\rho_{xy} = R_0 B + R_S \mu_0 M = \rho_{xy}^0 + \rho_{xy}^{AH}. \quad (1)$$

$R_0 = (en_{eff})^{-1}$ (n_{eff}: effective carrier density) and R_S are the ordinary and anomalous Hall coefficients, respectively, μ_0 the magnetic constant, M the magnetization, and $B = \mu_0[H + M(1 - N)]$, where the demagnetization factor N for thin films in a perpendicular magnetic field is $N \approx 1$. Hence $B = \mu_0 H$ and the Hall resistivity ρ_{xy} and Hall conductivity σ_{xy} can be written as

$$\rho_{xy} = R_0 \mu_0 H + S_H \rho^2 M, \quad (2)$$

$$\sigma_{xy} = \rho_{xy}/\rho^2 = R_0 \mu_0 H/\rho^2 + S_H M = \sigma_{xy}^0 + \sigma_{xy}^{AH}, \quad (3)$$

where $S_H = \mu_0 R_S/\rho^2$ and we have assumed $\rho_{xy} \ll \rho$. The above expressions are valid in weak magnetic fields for which $\omega_c \tau \ll 1$, where $\omega_c = eB/m$ is the cyclotron frequency, $\tau = m/ne^2\rho$ is the electron scattering time, and m is the effective electron mass.

For a particular system, R_0 may change with temperature due to the different contributions from several electronlike and holelike bands crossing the Fermi surface. The anomalous contribution σ_{xy}^{AH} contains an intrinsic contribution originating from the Berry-phase curvature correction to the group velocity of a Bloch electron induced by spin orbit interaction as well as extrinsic contributions arising from a side-jump mechanism and skew scattering [15]. The intrinsic contribution dominates the AHE in moderately conducting materials, while the skew scattering contribution is important at low temperatures and in clean samples of low impurity concentration. A scaling relation $\sigma_{xy} \propto \rho^{-\alpha}$ ($\alpha \geqslant 0$) has been proposed to cover the different transport regimes [30]. The conventional theories of the AHE derived via perturbation theory have shown $S_H \propto \lambda_{SO}$ independent of T, at least below the Curie temperature T_C [15,18]. The contributions from σ_{xy}^0 and σ_{xy}^{AH} can be disentangled by measuring the whole set of resistivities ρ_{xy} and ρ and the magnetization M in dependence of H and T.

II. EXPERIMENT

Thin polycrystalline $Mn_5Ge_3C_x$ ($x = 0$, 0.8) and $Mn_5Si_3C_{0.8}$ films were prepared by magnetron sputtering in high vacuum (base pressure $p < 10^{-4}$ Pa) from elemental targets at substrate temperatures $T_S = 400$–$470\,^{\circ}$C and were characterized by x-ray diffraction to confirm formation of the Mn_5Si_3-type structure as described earlier [12,13]. The films have a coarsely grained morphology with an average grain size equal to the film thickness. $(11\bar{2}0)$ oriented Al_2O_3 substrates covered by a mechanical mask were used to obtain a Hall-bar layout. For the samples investigated here, $w = 0.5$ mm, $d = 50$ nm ($Mn_5Ge_3C_x$) and 45 nm ($Mn_5Si_3C_{0.8}$), and $L = 8$ mm. Contacts to the sample were made by attaching thin Cu wires to the film, glued with silver epoxy. Resistivities were measured in a physical property measuring system (PPMS, Quantum Design) for magnetic fields $\mu_0 H$ up to ± 8 T and temperatures 2–400 K. The magnetic field was oriented either perpendicularly to the film plane or either longitudinally ($\rho_{\parallel,\mathrm{L}}$) or transverse ($\rho_{\parallel,\mathrm{T}}$) to the current direction in the film plane. The Hall resistivity ρ_{xy} was obtained by performing a field sweep from negative to positive values, $\rho_{xy} = [\rho_{xy}(+H) - \rho_{xy}(-H)]/2$.

The magnetic moment m of the films was measured in a superconducting quantum-interference device (SQUID) magnetometer between 10 and 350 K for magnetic fields up to 5 T. For the determination of the sample magnetization, in particular for temperatures close to T_C where the magnetization does not saturate in magnetic field, a correct subtraction of the diamagnetic signal of the Al_2O_3 substrate (volume V_s) is crucial. As an example, Fig. 2 shows $m(H)$ data of a $Mn_5Si_3C_{0.8}$ film on Al_2O_3 measured at 10 K before and after substraction of the diamagnetic contribution from the Al_2O_3 substrate. For the subtraction we have used the magnetic susceptibility χ of the substrate indicated by the red line in the inset of Fig. 2. χ was found to vary between -16.27×10^{-6} ($T = 10$ K) and -16.87×10^{-6} ($T \geqslant 150$ K). The red line is the average of various values $\chi = (\Delta m/\Delta H)/V_s$, determined from the slope $\Delta m/\Delta H$ of the linear $m(H)$ behavior above the saturation field at $T = 10$ K, for ferromagnetic films of Fe (squares), $Mn_5Si_3C_{0.8}$ (triangles), and $Mn_5Ge_3C_{0.8}$ (diamonds) on Al_2O_3 substrates. Solid circles represent data of Al_2O_3 reported by Smith *et al.* [31].

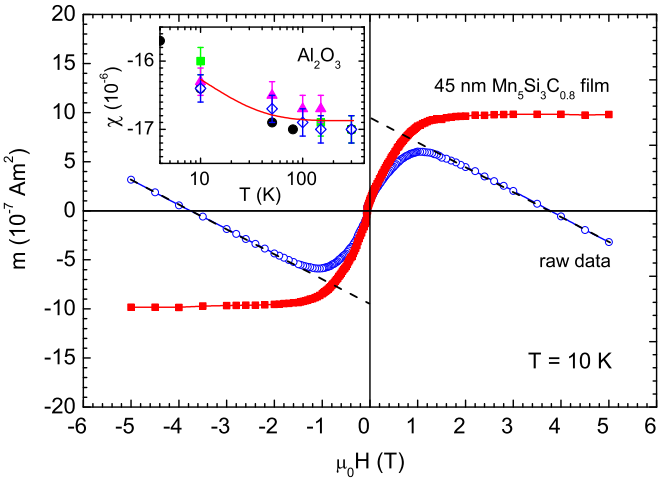

FIG. 2. (Color online) Magnetic moment m of a 45-nm $Mn_5Si_3C_{0.8}$ film (volume $V_f = 1.65 \times 10^{-6}$ cm^3) on a $(11\bar{2}0)$-oriented Al_2O_3 substrate (volume $V_s = 2 \times 10^{-2}$ cm^3) at $T = 10$ K in perpendicular magnetic field. Dashed lines indicate a linear $m \propto H$ behavior. Open symbols indicate raw data; closed symbols indicate the magnetic moment of the ferromagnetic film after the subtraction of the diamagnetic contribution arising from the substrate. Inset: temperature dependence of the magnetic susceptibility χ of Al_2O_3 in a semilogarithmic plot; see text for details.

III. RESULTS

The temperature dependence of the resistivity ρ for the three films is shown in Fig. 3. At low temperatures, the

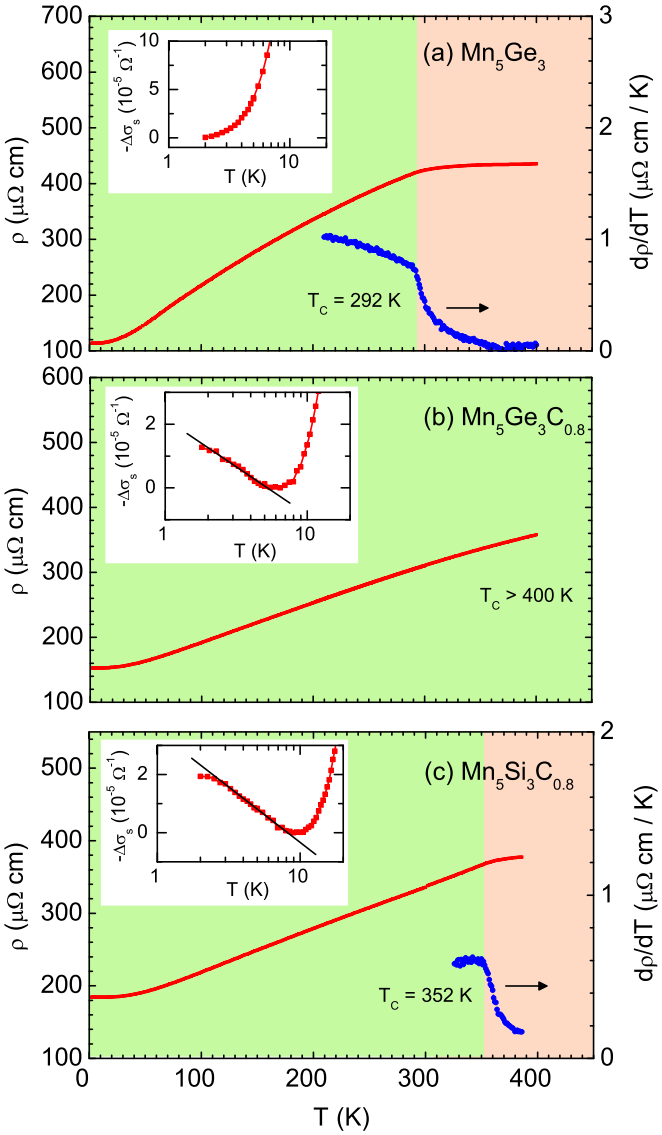

FIG. 3. (Color online) Temperature dependence of resistivity ρ (solid line) for ferromagnetic (a) Mn_5Ge_3, (b) $Mn_5Ge_3C_{0.8}$, and (c) $Mn_5Si_3C_{0.8}$ films. Kinks in $d\rho/dT$ in the vicinity of the Curie temperature T_C are shown in (a) and (c). Insets show a semilogarithmic plot of the variation of the sheet conductance $\Delta\sigma_s$ with T, where the solid line indicates a behavior $\Delta\sigma_s \propto \ln T$.

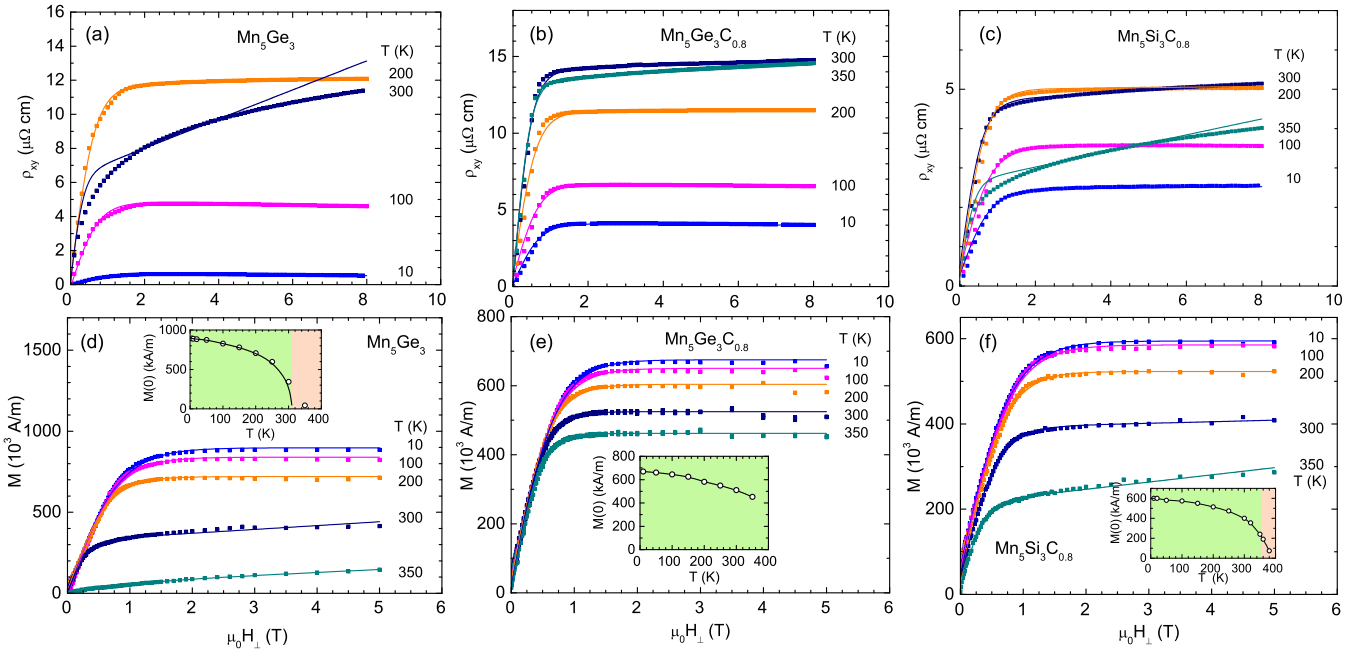

FIG. 4. (Color online) (a)–(c) Hall resistivity ρ_{xy} and (d)–(f) magnetization M in perpendicular field $H_\perp$ at various temperatures T. Solid lines show fits according to Eq. (2) to measured data (symbols); see text for details. Insets show the temperature dependence of the magnetization $M(0)$ obtained from the linear extrapolation of the high-field magnetization toward $H_\perp \to 0$.

films have residual resistivities ρ_0 (defined as the lowest resistivity of the sample) in the range 100–200 $\mu\Omega$ cm and exhibit at higher temperatures a roughly linear temperature dependence characteristic for a metal. At high temperatures, the slope of $\rho(T)$ changes and a weak kink appears at the Curie temperature T_C indicated in Figs. 3(a) and 3(c). This is not observed for $Mn_5Ge_3C_{0.8}$ consistent with a $T_C \approx 450$ K of this compound [7,9,11], which was not accessible by the experimental setup used in this study. The magnetic phase transitions are better resolved in the derivative $d\rho/dT$; see Figs. 3(a) and 3(c), which shows a clear jump at T_C [32]. The T_C values determined from $d\rho/dT$ are in very good agreement with earlier published data for Mn_5Ge_3 [5] and $Mn_5Si_3C_{0.8}$ films [12,13].

The insets of Fig. 3 show the sheet conductance $\Delta\sigma_s = [\rho_0 - \rho]d/\rho_0^2$ vs $\ln T$ for temperatures $T < 10$ K. For the C-inserted films [Figs. 3(b) and 3(c)] a behavior $-\Delta\sigma_s \propto -\ln T$ is observed (solid lines) where $\Delta\sigma_s$ varies a few $10^{-5}\Omega^{-1}$ over one decade of temperature. This has been observed earlier for $Mn_5Si_3C_{0.8}$ films [13] and was attributed to the scattering of conduction electrons by two-level systems originating from structural disorder, possibly with a crossover to Fermi-liquid behavior below $\approx$1 K. In the present case, the logarithmic T dependence is not observed for Mn_5Ge_3 [Fig. 3(a)] which suggests that the disorder in the $Mn_5Si_3C_{0.8}$ and $Mn_5Ge_3C_{0.8}$ films is induced by the insertion of carbon into the crystalline lattice.

Due to the high residual resistivities ρ_0 and low residual resistance ratios $RRR = \rho(300\ \mathrm{K})/\rho_0 \approx 2$–4 the films fall into the intrinsic Hall-effect regime [30]. From $\rho_0 l = 4.25 \times 10^{-15}\Omega\,\mathrm{m}^2$ for Mn_5Ge_3 [33] an electron mean free path $l \approx 3$ nm is estimated, much smaller than the film thickness. Therefore, finite-size effects arising from electron scattering at the film boundaries are considered to be negligible. Furthermore, the cyclotron resonance frequency is $\omega_c\tau = R_0 B/\rho \approx 10^{-4} B(\mathrm{T}) \ll 1$ and the weak-field expressions (no closed orbits) Eqs. (2) and (3) are applicable.

Figures 4(a)–4(c) show the Hall resistivity ρ_{xy} vs magnetic field H for different T. For clarity, only a subset of data is shown. ρ_{xy} of the ferromagnetic films shows a steep increase with field at low fields and a saturation at high fields for $T \ll T_C$, resembling the behavior of the magnetization M vs field H; see Figs. 4(d)–4(f). We do not observe a nonlinear behavior of $\rho_{xy}(H)$ or a sign change with magnetic field that would allow a separation of electron and hole contributions [34]. This indicates that field-induced changes of particular orbits or a reconstruction of the Fermi surface are negligible as expected in the weak-field regime $\omega\tau \ll 1$. In perpendicular magnetic field, the magnetization exhibits a hard-axis behavior without hysteresis due to the strong shape anisotropy of the thin film. For all films the magnetization $M(0)$, determined by extrapolating the high-field behavior of M to $H = 0$, shows the characteristic dependence of a ferromagnet (see insets). $M(0)$ of Mn_5Ge_3 and $Mn_5Si_3C_{0.8}$ is zero at T_C obtained from the jump in $d\rho/dT$. T_C of $Mn_5Ge_3C_{0.8}$ is higher than 400 K. For $Mn_5Si_3C_{0.8}$ we obtain at $T = 10$ K a saturation magnetization $M_S = 6 \times 10^5$ A/m corresponding to a magnetic moment of $1.3\mu_B$/Mn, somewhat higher than $1\mu_B$/Mn observed earlier for sputtered 100-nm $Mn_5Si_3C_{0.8}$ films [13] but similar to $1.2\mu_B$/Mn of 400-nm-thick C-implanted $Mn_5Si_3C_{0.8}$ films [29]. For $Mn_5Ge_3C_{0.8}$, $M_S = 6.7 \times 10^5$ A/m ($1.6\mu_B$/Mn), 27% lower than for 400-nm-thick implanted films ($2.2\,\mu_B$/Mn) [29]. For the Mn_5Ge_3 film we obtain $M_S = 9 \times 10^5$ A/m ($2.1\mu_B$/Mn), 20% lower than M_S of bulk Mn_5Ge_3 ($2.6\mu_B$/Mn). We attribute the differences in the values to the uncertainty in the determination

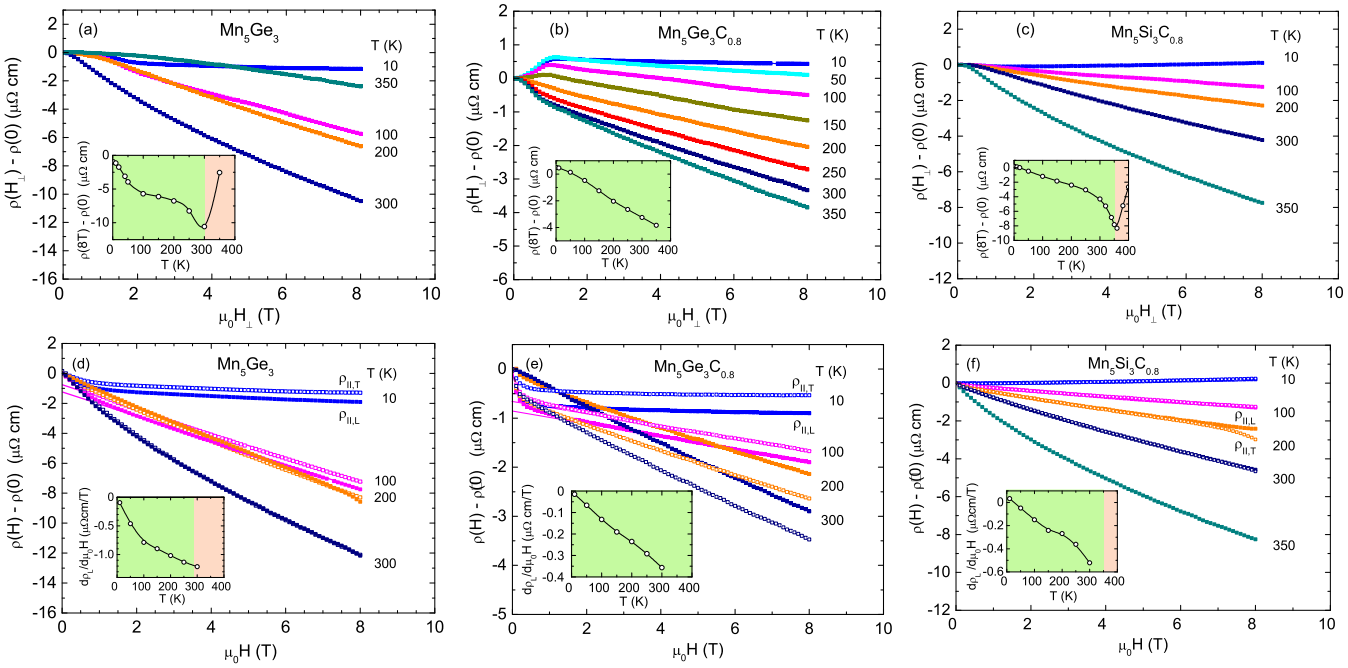

FIG. 5. (Color online) (a)–(c) Magnetoresistivity in perpendicular magnetic field $H_\perp$ for various temperatures T. Insets show the temperature dependence of $\rho(8\ \mathrm{T}) - \rho(0)$. (d)–(f) $\rho(H)$ with the magnetic field oriented in the plane and either longitudinal ($\rho_{\parallel,\mathrm{L}}$, closed symbols) or transverse ($\rho_{\parallel,\mathrm{T}}$, open symbols) to the direction of the current. Insets show temperature dependence of the nearly linear slope $d\rho_{\parallel,\mathrm{L}}/(d\mu_0 H)$ of the longitudinal MR. Solid lines indicate the extrapolation of the MR to zero field for the determination of the AMR ratio.

of the film volume and to slight deviations of the composition from the stoichiometric ratio for samples prepared in different runs. In addition, the presence of a magnetically disordered layer close to the substrate/film interface might lead to a reduced magnetic moment which is more pronounced in thin than in thick films.

The magnetoresistance (MR) is negative for all temperatures as shown in Fig. 5, except for $Mn_5Ge_3C_{0.8}$ where a small positive MR is observed in a weak perpendicular magnetic field at temperatures $T \leqslant 150$ K. Changes of the MR at low fields $\mu_0 H < 1$ T are attributed to a change of the magnetic domain structure. In perpendicular field, $\rho(8\ \mathrm{T}) - \rho(0)$ varies with temperature; see insets Figs. 5(a)–5(c). $\rho(8\ \mathrm{T}) - \rho(0)$ decreases with increasing temperature all the way up to T_C and increases again with a distinct minimum at T_C observed in Figs. 5(a) and 5(c). The negative MR in perpendicular field was reported earlier for $Mn_5Si_3C_{0.8}$ [13] and was attributed to the damping of spin waves by the magnetic field [35]. In a high magnetic field a gap opens in the magnon spectrum and the electron-magnon scattering is suppressed leading to a decrease of the resistivity. Close to T_C, the MR shows a nonlinear behavior, MR $\propto H^{2/3}$ for $T < T_\mathrm{C}$ and MR $\propto H^\alpha$ with $\alpha = 1.8$–1.9 for $T > T_\mathrm{C}$, for $Mn_5Si_3C_{0.8}$ and Mn_5Ge_3 as shown in Fig. 6 where the MR is plotted vs $H^{2/3}$. This is in qualitative agreement with a simple model where a localized spin system is approximated by a molecular field and the MR is due to s-d scattering [36].

For Mn_5Ge_3 and $Mn_5Ge_3C_{0.8}$ we observe differences between the longitudinal and transverse MR with the field oriented in the plane of the film; see Figs. 5(d) and 5(e) arising from AMR. In contrast, no AMR is observed for $Mn_5Si_3C_{0.8}$ [Fig. 5(f)]. For all samples, orbital contributions to $\rho_{\parallel,\mathrm{L}} \propto (\omega_c \tau)^2 \propto \mu H^2$ are negligibly small (μ: mobility; see below) [37]. From $\rho_{\parallel,\mathrm{L}}$ and $\rho_{\parallel,\mathrm{T}}$ we determine the AMR ratio $(\rho_{\parallel,\mathrm{L}} - \rho_{\parallel,\mathrm{T}})/\rho_{\parallel,\mathrm{T}}$ plotted in Fig. 7(a). While no AMR is observed for $Mn_5Si_3C_{0.8}$ independent of temperature, the negative AMR ratio of Mn_5Ge_3 and $Mn_5Ge_3C_{0.8}$ at low temperature increases with increasing temperature up to positive values at high temperatures thereby crossing zero around 150–200 K. At $T = 300$ K the AMR ratio of Mn_5Ge_3 is zero because the temperature is higher than T_C. The different temperature dependence of the AMR ratio of $Mn_5Ge_3C_x$ and $Mn_5Si_3C_{0.8}$ will be discussed in Sec. IV. The insets in Figs. 5(d)–5(f) show that the slope $d\rho/dH$ continuously decreases with increasing T, similar to $\rho(8\ \mathrm{T}) - \rho(0)$ in perpendicular magnetic field [insets Figs. 5(a)–5(c)].

With the data of Figs. 4 and 5 we are able to separate the different contributions to the Hall effect. We apply Eqs. (2) and (3) to analyze the AHE of the ferromagnetic films. In Fig. 8(a), $\sigma_{xy}^{\mathrm{AH}} = (\rho_{xy} - R_0 \mu_0 H)/\rho^2$ at different T is plotted vs M for $Mn_5Ge_3C_{0.8}$ as an example; cf. Eq. (3). For clarity, again only a subset of data is shown. R_0 was used as a free parameter to yield a linear behavior $\sigma_{xy}^{\mathrm{AH}} = S_H M$ crossing the origin [38]. This assumption is derived from the linear dependence $\sigma_{xy}^{\mathrm{AH}} \propto M$ reported earlier for epitaxial Mn_5Ge_3 films on Ge(111) and attributed to the existence of long-wavelength spin fluctuations in this material [39]. R_0 can be determined with sufficient accuracy because small variations of R_0 drastically change the $\sigma_{xy}^{\mathrm{AH}} \propto M$ behavior, in particular above the saturation field; see inset Fig. 8(a). A variation of $R_0 = 1.5 \times 10^{-10}$ m^3/As by $\pm 5 \times 10^{-11}$ m^3/As gives rise to a strong deviation of the data from the $\sigma_{xy}^{\mathrm{AH}} \propto M$ behavior for high values of M. The influence of the MR on the Hall effect cancels by this procedure. We obtain the Hall coefficients R_0

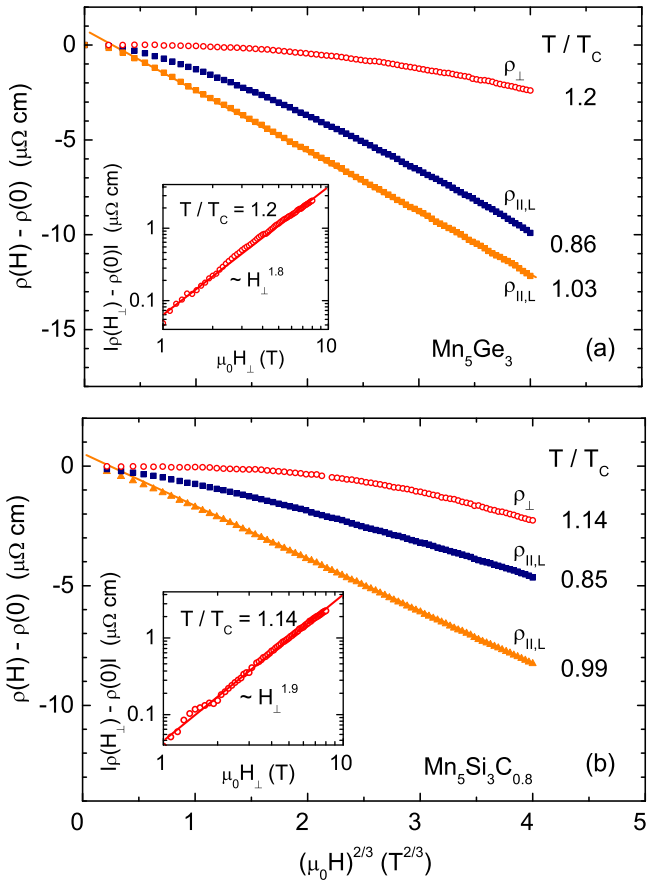

FIG. 6. (Color online) MR of (a) Mn_5Ge_3 ($T_C = 292$ K) and (b) $Mn_5Si_3C_{0.8}$ ($T_C = 352$ K) vs $H^{2/3}$ for temperatures close to T_C. T_C could not be reached for $Mn_5Ge_3C_{0.8}$. $\rho_\perp$ indicates data measured in perpendicular field and $\rho_{\parallel,L}$ the longitudinal MR with the field in the plane. Insets show double-logarithmic plots of the MR vs perpendicular magnetic field $H_\perp$ just above T_C. Solid lines indicate a power-law behavior.

and S_H from the slope of σ_{xy}^{AH} [Fig. 8(a)] allowing calculation of the Hall resistivity ρ_{xy} [Eq. (2)] for comparison with the experimental data. We obtain good agreement between the measured Hall resistivity and the calculated values, see Figs. 4(a)–4(c), except for temperatures close to T_C. We mention that similar values for R_0 and S_H are obtained from a plot $\rho_{xy}/\mu_0 H$ vs $\rho^2 M/\mu_0 H$. Moreover, adding a contribution $\propto\rho$ due to skew scattering to the Hall effect does not improve the agreement between the measured and calculated values. This is due to the fact that the resistivities of the polycrystalline films are high and the Hall effect is dominated by the contributions $\propto\rho^2$ [15,30].

The temperature dependence of the coefficient S_H of the anomalous Hall effect is plotted in Fig. 8(b). For all three films, S_H is positive and T independent almost up to T_C due to $S_H \propto \lambda_{SO}$ as observed earlier [15,18,39]. S_H only gradually decreases close to T_C but a finite S_H is still observed in the paramagnetic regime above T_C presumably due to the T-independent spin-orbit interaction λ_{SO} [18,40]. λ_{SO} can be roughly estimated from the dimensionless coupling for d orbitals of size $r_d \approx 0.05$ nm ($Ze^2/2\epsilon_0 mc^2 r_d$) and the band kinetic energy ($\hbar^2/2ma^2$) [41]. For $Z_{Mn} = 25$, $a = 0.5$ nm we obtain $\lambda_{SO} \approx 0.1$ meV (1.2 K). S_H successively increases from Mn_5Ge_3, $Mn_5Si_3C_{0.8}$, to $Mn_5Ge_3C_{0.8}$, possibly due to the increasing ferromagnetic stability. This is supported by a linear increase of $S_H(T \to 0)$ with T_C of the samples shown in the inset of Fig. 8(b).

For $Mn_5Si_3C_{0.8}$, the ordinary Hall coefficient $R_0 \approx 2 \times 10^{-10}$ m^3/A s is positive and independent of temperature, and corresponds to an effective charge carrier density $n_{eff} = |1/R_0 e| = 3 \times 10^{22}$ cm^{-3}, i.e., a factor of 5 higher than for Mn_5Si_3 ($n_{eff} = 6 \times 10^{21}$ cm^{-3}) [23], suggesting p-type doping by carbon; see Fig. 7(b). This can be due to a carbon-induced change of the electronic band structure and an increased density of states at the Fermi level, similar to what has been found for $Mn_5Ge_3C_x$ [8]. From R_0 and ρ_0 we obtain a Hall mobility $\mu = |R_0|/\rho_0 = 1.1$ cm^2/V s.

In contrast, the ordinary Hall coefficient R_0 for the $Mn_5Ge_3C_x$ films strongly varies with temperature; see Fig. 7(b). In particular, $R_0 = -2 \times 10^{-10}$ m^3/A s is negative at $T = 10$ K for both $Mn_5Ge_3C_x$ films yielding $n_{eff} = 3 \times 10^{22}$ cm^{-3} corresponding to $\approx$0.8 electrons per Mn and a Hall mobility $\mu = 2$ cm^2/V s. The low Hall mobilities for all samples confirm our statement above that the orbital contribution to $\rho_{\parallel,L}$ is small [37]. R_0 of both $Mn_5Ge_3C_x$ films increases $\propto T^2$ and changes sign around 120 K indicating an increasing contribution from holelike bands. We note that R_0 vs T/T_C obeys a similar behavior for both $Mn_5Ge_3C_x$ samples. The temperature dependence of R_0 is in agreement with the behavior of epitaxially grown Mn_5Ge_3 films, where $R_0 \approx -3 \times 10^{-10}$ m^3/A s was obtained at low temperature with a sign change from negative to positive at 180 K [39]. A sign change of R_0 was also reported for nonmagnetic $CaRuO_3$ and ferromagnetic $SrRuO_3$ films and was attributed to the zero band curvature of the Fermi surfaces in these materials [42].

IV. DISCUSSION

The resistivity, magnetoresistance, and Hall effect of all samples clearly show the characteristic features of a ferromagnetic metal, i.e., a kink in $d\rho/dT$ at T_C, a temperature-dependent MR, and an anomalous Hall effect much larger than the ordinary Hall effect. However, both $Mn_5Ge_3C_x$ films show a qualitatively different temperature dependence of the AMR and ordinary Hall coefficient R_0 compared to the $Mn_5Si_3C_{0.8}$ film, although all compounds have the same hexagonal crystal structure. In particular, for $Mn_5Ge_3C_x$ both coefficients, AMR and R_0, show a sign change in a similar tempüerature range. The difference in the temperature dependences presumably arises from the substantially different electronic band structure in the vicinity of E_F of $Mn_5Si_3C_{0.8}$ and $Mn_5Ge_3C_x$, which seems to be independent of C doping in the case of $Mn_5Ge_3C_x$. This might originate from the different lattice constants and the different atomic configuration of the constituents Si and Ge. The volume of the crystallographic unit cell increases continuously from $Mn_5Si_3C_{0.8}$ to $Mn_5Ge_3C_{0.8}$ to Mn_5Ge_3 [14] in line with an increasing temperature dependence of R_0. The sensitivity of the magnetic moment and the spin polarization, i.e., spin-split band structure, to interatomic distances and strain in Mn_5Ge_3 has been reported earlier [27,33,43].

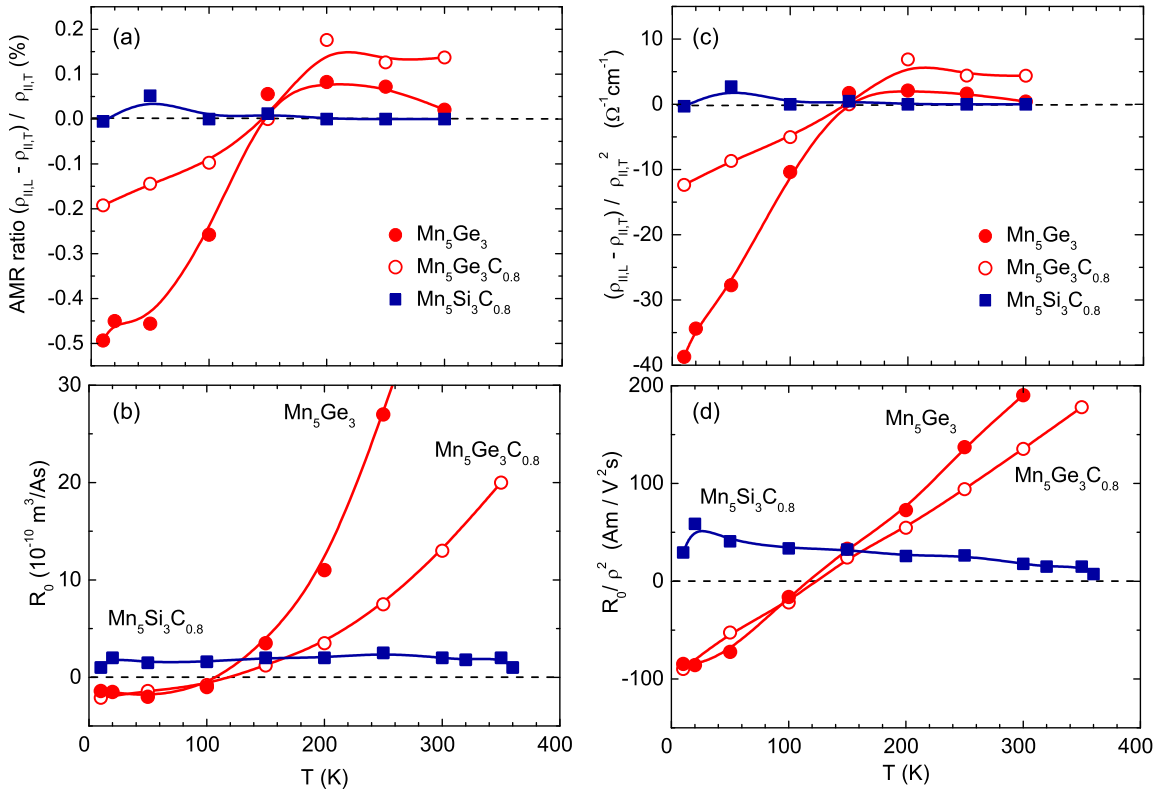

FIG. 7. (Color online) (a),(b) Temperature dependence of the AMR ratio and of the ordinary Hall coefficient R_0, respectively, for Mn_5Ge_3 (closed circles), $Mn_5Ge_3C_{0.8}$ (open circles), and $Mn_5Si_3C_{0.8}$ (squares). (c) and (d) show $(\rho_{\parallel,L} - \rho_{\parallel,T})/\rho_{\parallel,T}^2$ and the reduced Hall coefficient R_0/ρ^2, respectively.

In the following we propose a scenario for the concomitant sign changes of the AMR ratio and Hall coefficient R_0 in $Mn_5Ge_3C_x$ films. In the two-current model for strong ferromagnets, the size of the AMR depends on the intraband scattering of conduction electrons by nonmagnetic impurities and on the scattering of conduction electrons into the unoccupied states of the $d_\downarrow$ band close to the Fermi level E_F [17,44]. The AMR is often positive while a negative AMR as observed in Fe_4N has been taken as evidence for minority-spin conduction [45]. In this context, the two-current model has been extended to take into account (i) scattering into unoccupied d states of *both* spin components, (ii) spin mixing of the d bands by spin-orbit scattering, and (iii) spin-flip scattering arising from spin-dependent disorder and magnons [46]. In the extended two-current model $\rho_{s\uparrow}$ and $\rho_{s\downarrow}$ denote the resistivities of the conducting s, p, and d states with spin up ($\uparrow$) or down ($\downarrow$), respectively, arising from scattering by nonmagnetic impurities. The ratio $\rho_{s\downarrow}/\rho_{s\uparrow}$ is treated as a variable together with the spin-resolved components of the d-band DOS at E_F, $N_\downarrow^d$, and $N_\uparrow^d$. $\rho_{s\to d\zeta}$ denotes the resistivity due to s-d scattering in which the conduction electron is scattered into localized d states of spin ζ by impurities. The AMR ratio arises from slight changes of the d orbitals by the spin-mixing term due to spin-orbit interaction. Interestingly, the sign of the AMR ratio does not depend on the absolute value of spin-flip scattering rate but on the ratios $\rho_{s\downarrow}/\rho_{s\uparrow}$, $N_\downarrow^d/N_\uparrow^d$, and the dominant s-d scattering process [46].

The DOS of the spin-split band structure of Mn_5Ge_3 and $Mn_5Ge_3C_{0.8}$ has been obtained from first-principle calculations [8,33,47]. At the Fermi level, the total DOS $N(E_F)$ is dominated by $N^d(E_F)$ of the Mn_1 and Mn_2 d states with a lower $N_\uparrow^d$ than $N_\downarrow^d$. The Ge and C p bands do not contribute to the transport directly, but the Mn states in the majority spin band are strongly hybridized with the Ge $4p$ states. Similarly, the C $2p$ states hybridize with the Mn_2 states leading to a shift of the Mn_2 peaks in the DOS towards E_F and to an increased $N^d(E_F)$ in both spin channels, while the Mn_1 states are left almost unaffected [8]. The calculations yield $N_\downarrow/N_\uparrow \approx N_\downarrow^d/N_\uparrow^d \approx 1.5$–$2$ at E_F and an exchange splitting $E_{ex} \approx 2.5$ eV [8,33,47]. By using $1/\rho_{s\uparrow(\downarrow)} \approx e^2 N_{\uparrow(\downarrow)}(E_F)\langle v_{F\uparrow(\downarrow)}\rangle^2 \tau$ with the appropriate values given in Refs. [8,33] we obtain $\rho_{s\downarrow}/\rho_{s\uparrow} \approx 0.3$ at low temperatures, i.e., a higher conductivity of the minority-spin channel, akin to Fe_4N [45]. A similar $\rho_{s\downarrow}/\rho_{s\uparrow}$ value is derived from the spin polarization $P = -0.42$ measured by Andreev reflection [33]. For $\rho_{s\downarrow}/\rho_{s\uparrow} \approx 0.3$ we obtain in the extended two-current model [46] a negative AMR ratio $= -0.3\%$ for a dominant s-d scattering contribution $\rho_{s\to d\downarrow}/\rho_{s\uparrow} = 0.2$. The maximum negative AMR ratio is usually of the order of $-\gamma = -\frac{3}{4}(\lambda_{SO}/E_{ex})^2 = -1\%$ as found experimentally, corresponding to $\lambda_{SO} = 0.3$ eV in the present case, which is in fair agreement with the rough estimate mentioned above [41].

The Hall constant in the two-current model is $R_0/\rho_0^2 = (R_{0\uparrow}/\rho_\uparrow^2 + R_{0\downarrow}/\rho_\downarrow^2)$, where $R_{0\downarrow}$ and $R_{0\uparrow}$ are the temperature independent ordinary Hall coefficients of the spin down and spin up band, respectively, and $\rho_\downarrow$ and $\rho_\uparrow$ are the total resistivities of the spin-split bands. Due to the metallic character of the material and the linear $\rho(T)$ dependence, see

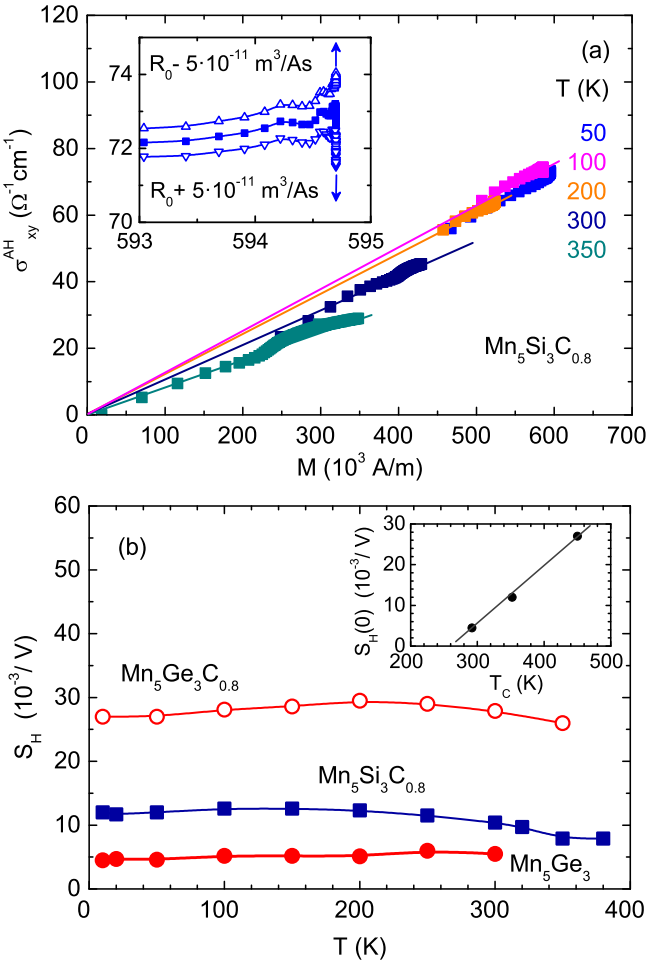

FIG. 8. (Color online) (a) Anomalous contribution σ_{xy}^{AH} vs M for $Mn_5Si_3C_{0.8}$. Colors indicate different temperatures; cf. Figs. 4 and 5. Solid lines indicate a linear behavior $\sigma_{xy}^{AH} \propto M$. Inset shows the effect of a variation of the Hall coefficient R_0 on the σ_{xy}^{AH} vs M behavior at large M for $T = 50$ K. (b) Temperature dependence of the anomalous Hall coefficient S_H. Inset shows the dependence of $S_H(0)$ for $T \to 0$ from the Curie temperature T_C. Solid line indicates a linear behavior.

Fig. 2, it is reasonable to assume temperature-independent carrier densities $n_\downarrow$ and $n_\uparrow$ and, hence, constant $R_{0\downarrow}$ and $R_{0\uparrow}$.

From the AMR of $Mn_5Ge_3C_x$ at low T we know that the $\downarrow$ channel dominates the transport ($\rho_\downarrow \ll \rho_\uparrow$) and $R_0 < 0$ requires $R_{0\downarrow} < 0$. At higher temperatures $R_0 > 0$ requires $R_{0\uparrow} > 0$ and $\rho_\downarrow > \rho_\uparrow$. Hence $\rho_\downarrow/\rho_\uparrow$ must increase with T in order to induce a sign change of the AMR *and* R_0. The change from an electronlike minority-spin transport to a holelike majority-spin transport in $Mn_5Ge_3C_x$ is possible since in a ferromagnetic metal electrons of one spin direction may constitute an electronlike Fermi surface, while electrons of opposite sign may constitute a holelike surface [48].

From the extended two-current model an increase of $\rho_\downarrow/\rho_\uparrow$ with increasing temperature can be due to an increase of $\rho_{s\downarrow}/\rho_{s\uparrow}$ and/or of $N^d_\uparrow/N^d_\downarrow$ [46]. The latter has been proposed as an explanation for the AMR sign change in the half-metallic ferromagnet Fe_3O_4 with spin-split t_{2g} and e_g states [46,49]. However, negative as well as positive ordinary Hall coefficients have been reported for Fe_3O_4 in the range 160 K $< T <$ 300 K [50,51]. In half-metallic CrO_2 the electrons determine the conductivity while highly mobile holes determine the low-field magnetotransport properties [34]. In the present case of conductive s, p, and d states it is likely that the strong hybridization between the Mn $3d$ states and the Ge states changes the conductivity of the spin-split conduction channels. This seems not to be the case for $Mn_5Si_3C_{0.8}$.

V. SUMMARY

We have investigated the Hall effect and anisotropic magnetoresistance of ferromagnetic Mn_5Ge_3, $Mn_5Ge_3C_{0.8}$, and $Mn_5Si_3C_{0.8}$ films. While for $Mn_5Si_3C_{0.8}$ the Hall coefficients are roughly independent of temperature, for $Mn_5Ge_3C_x$ these coefficients show a concomitant sign change from negative to positive in the same range of T. This could be due to the fact that the electronic and magnetic properties in these Mn compounds depend very sensitively on the interatomic distances and the atomic environment around the magnetic Mn ions. Calculations of the band structure and electronic transport properties are strongly required in the future to confirm this hypothesis. In addition, we have demonstrated a clear relation between the temperature dependence of the Hall coefficient and anisotropic magnetoresistance. Further work should show if this relation holds for other classes of ferromagnetic transition-metal compounds as well. We conclude that these results have to be taken into account when considering the implementation of $Mn_5Si_3C_x$ or $Mn_5Ge_3C_x$ as ferromagnetic electrodes for spin injection and detection in spintronic applications based on, e.g., Si or Ge heterostructures.

ACKNOWLEDGMENTS

We gratefully acknowledge financial support from the Deutsche Forschungsgemeinschaft through the Center for Functional Nanostructures (CFN). We thank I. A. Fischer for valuable discussions.

[1] S. A. Wolf, D. D. Awschalom, R. A. Buhrman, J. M. Daughton, S. von Molnár, M. L. Roukes, A. Y. Chtchelkanova, and D. M. Treger, Science **294**, 1488 (2001).

[2] I. Žutić, J. Fabian, and S. Das Sarma, Rev. Mod. Phys. **76**, 323 (2004).

[3] R. Jansen, Nat. Mater. **11**, 400 (2012).

[4] Y. Zhou, W. Han, L.-T. Chang, F. Xiu, M. Wang, M. Oehme, I. A. Fischer, J. Schulze, R. K. Kawakami, and K. L. Wang, Phys. Rev. B **84**, 125323 (2011).

[5] C. Zeng, S. C. Erwin, L. C. Feldman, A. P. Li, R. Jin, Y. Song, J. R. Thompson, and H. H. Weitering, Appl. Phys. Lett. **83**, 5002 (2003).

[6] K. Kanematsu, J. Phys. Soc. Jpn. **17**, 85 (1962).
[7] M. Gajdzik, C. Sürgers, M. Kelemen, and H. v. Löhneysen, J. Magn. Magn. Mater. **221**, 248 (2000).
[8] I. Slipukhina, E. Arras, P. Mavropoulos, and P. Pochet, Appl. Phys. Lett. **94**, 192505 (2009).
[9] A. Spiesser, I. Slipukhina, M.-T. Dau, E. Arras, V. Le Thanh, L. Michez, P. Pochet, H. Saito, S. Yuasa, M. Jamet *et al.*, Phys. Rev. B **84**, 165203 (2011).
[10] I. A. Fischer, J. Gebauer, E. Rolseth, P. Winkel, L.-T. Chang, K. L. Wang, C. Sürgers, and J. Schulze, Semicond. Sci. Technol. **28**, 125002 (2013).
[11] V. L. Thanh, A. Spiesser, M.-T. Dau, S. F. Olive-Mendez, L. A. Michez, and M. Petit, Adv. Nat. Sci.: Nanosci. Nanotechnol. **4**, 043002 (2013).
[12] C. Sürgers, M. Gajdzik, G. Fischer, H. v. Löhneysen, E. Welter, and K. Attenkofer, Phys. Rev. B **68**, 174423 (2003).
[13] B. Gopalakrishnan, C. Sürgers, R. Montbrun, A. Singh, M. Uhlarz, and H. v. Löhneysen, Phys. Rev. B **77**, 104414 (2008).
[14] C. Sürgers, K. Potzger, and G. Fischer, J. Chem. Sci. **121**, 173 (2009).
[15] N. Nagaosa, J. Sinova, S. Onoda, A. H. MacDonald, and N. P. Ong, Rev. Mod. Phys. **82**, 1539 (2010).
[16] T. McGuire and R. Potter, IEEE Trans. Magn. **11**, 1018 (1975).
[17] I. A. Campbell and A. Fert, in *Ferromagnetic Materials*, edited by E. P. Wohlfarth (North-Holland, Amsterdam, 1982), Vol. 3.
[18] Z. Fang, N. Nagaosa, K. S. Takahashi, A. Asamitsu, R. Mathieu, T. Ogasawara, H. Yamada, M. Kawasaki, Y. Tokura, and K. Terakura, Science **302**, 92 (2003).
[19] *International Tables of Crystallography*, Vol. A, edited by T. Hahn (Reidel, Dordrecht, 1983).
[20] P. J. Brown, J. B. Forsyth, V. Nunez, and F. Tasset, J. Phys.: Condens. Matter **4**, 10025 (1992).
[21] P. J. Brown and J. B. Forsyth, J. Phys.: Condens. Matter **7**, 7619 (1995).
[22] M. Gottschilch, O. Gourdon, J. Persson, C. de la Cruz, V. Petricek, and T. Brueckel, J. Mater. Chem. **22**, 15275 (2012).
[23] C. Sürgers, G. Fischer, P. Winkel, and H. v. Löhneysen, Nat. Commun. **5**, 3400 (2014).
[24] J.-P. Sénateur, J.-P. Bouchaud, and R. Fruchart, Bull. Soc. Fr. Mineral. Cristallogr. **90**, 537 (1967).
[25] M. Gajdzik, C. Sürgers, M. Kelemen, and H. v. Löhneysen, J. Appl. Phys. **87**, 6013 (2000).
[26] C. Sürgers, H. v. Löhneysen, M. Kelemen, E. Dormann, and M. Brooks, J. Magn. Magn. Mater. **240**, 383 (2002).
[27] J. B. Forsyth and P. J. Brown, J. Phys.: Condens. Matter **2**, 2713 (1990).
[28] A. Stroppa and M. Peressi, Phys. Status Solidi A **204**, 44 (2007).
[29] C. Sürgers, K. Potzger, T. Strache, W. Möller, G. Fischer, N. Joshi, and H. v. Löhneysen, Appl. Phys. Lett. **93**, 062503 (2008).
[30] S. Onoda, N. Sugimoto, and N. Nagaosa, Phys. Rev. B **77**, 165103 (2008).
[31] A. R. Smith, D. J. Arnold, and R. W. Mires, Phys. Rev. B **2**, 2323 (1970).
[32] F. C. Zumsteg and R. D. Parks, Phys. Rev. Lett. **24**, 520 (1970).
[33] R. P. Panguluri, C. Zeng, H. H. Weitering, J. M. Sullivan, S. C. Erwin, and B. Nadgorny, Phys. Status Solidi B **242**, R67 (2005).
[34] S. M. Watts, S. Wirth, S. von Molnar, A. Barry, and J. M. D. Coey, Phys. Rev. B **61**, 9621 (2000).
[35] B. Raquet, M. Viret, E. Sondergard, O. Cespedes, and R. Mamy, Phys. Rev. B **66**, 024433 (2002).
[36] H. Yamada and S. Takada, J. Phys. Soc. Jpn. **34**, 51 (1973).
[37] N. A. Porter, J. C. Gartside, and C. H. Marrows, Phys. Rev. B **90**, 024403 (2014).
[38] W. Jiang, X. Z. Zhou, and G. Williams, Phys. Rev. B **82**, 144424 (2010).
[39] C. Zeng, Y. Yao, Q. Niu, and H. H. Weitering, Phys. Rev. Lett. **96**, 037204 (2006).
[40] G. Tatara and H. Kawamura, J. Phys. Soc. Jpn. **71**, 2613 (2002).
[41] J. Ye, Y. B. Kim, A. J. Millis, B. I. Shraiman, P. Majumdar, and Z. Tešanović, Phys. Rev. Lett. **83**, 3737 (1999).
[42] S. C. Gausepohl, M. Lee, R. A. Rao, and C. B. Eom, Phys. Rev. B **54**, 8996 (1996).
[43] D. D. Dung, D. Odkhuu, L. T. Vinh, S. C. Hong, and S. Cho, J. Appl. Phys. **114**, 073906 (2013).
[44] I. A. Campbell, A. Fert, and O. Jaoul, J. Phys. C: Solid State Phys. **3**, S95 (1970).
[45] M. Tsunoda, Y. Komasaki, S. Kokado, S. Isogami, C.-C. Chen, and M. Takahashi, Appl. Phys. Express **2**, 083001 (2009).
[46] S. Kokado, M. Tsunoda, K. Harigaya, and A. Sakuma, J. Phys. Soc. Jpn. **81**, 024705 (2012).
[47] A. Stroppa, G. Kresse, and A. Continenza, Appl. Phys. Lett. **93**, 092502 (2008).
[48] W. A. Reed and E. Fawcett, Science **146**, 603 (1964).
[49] M. Ziese, Phys. Rev. B **62**, 1044 (2000).
[50] D. Reisinger, P. Majewski, M. Opel, L. Alff, and R. Gross, Appl. Phys. Lett. **85**, 4980 (2004).
[51] K. Siratori, S. Todo, and S. Kimura, J. Phys. Soc. Jpn. **57**, 2093 (1988).
[52] L. Castelliz, Mon. Chem. Teil. Wiss. **84**, 765 (1953).
[53] T. Wolz, C. Sürgers, and H. v. Löhneysen (unpublished).